

Nanoparticle-induced light scattering for improved performance of quantum-well solar cells

D. Derkacs, W. V. Chen, P. M. Matheu,^{a)} S. H. Lim, P. K. L. Yu, and E. T. Yu^{b)}
 Department of Electrical and Computer Engineering, University of California, San Diego, La Jolla,
 California 92093-0407, USA

(Received 22 June 2008; accepted 1 August 2008; published online 3 September 2008)

We report on the improved performance of InP/InGaAsP quantum-well waveguide solar cells via light scattering from deposited dielectric or metal nanoparticles. The integration of metal or dielectric nanoparticles above the quantum-well solar cell device is shown to couple normally incident light into lateral optical propagation paths, with optical confinement provided by the refractive index contrast between the quantum-well layers and surrounding material. With minimal optimization, short-circuit current density increases of 12.9% and 7.3% and power conversion efficiency increases of 17% and 1% are observed for silica and Au nanoparticles, respectively.

© 2008 American Institute of Physics. [DOI: 10.1063/1.2973988]

There is currently intense interest in the application of semiconductor nanostructures, including quantum-well structures,¹ nanowires,² and quantum dots³ in photovoltaic devices capable of operation at power conversion efficiencies that exceed the theoretical single-junction limit of 31%.⁴ In quantum-well solar cells, for which maximum predicted theoretical power conversion efficiencies range from 44.5% (Ref. 1) to over 63%,⁵ the tradeoff between incorporation of a sufficient number of quantum wells to ensure high photon absorption efficiency and increased short-circuit current density (J_{sc}) and the resulting reduction in open-circuit voltage (V_{oc}) due to less-than-unity efficiency collection of photogenerated carriers is especially problematic.⁶ Despite this difficulty, the resulting maximum power delivered for a quantum-well solar cell device can exceed that of a corresponding homojunction device by extending the absorption spectrum to longer wavelengths.^{6,7} We show here that normally incident light can be coupled into lateral optical propagation paths within the quantum-well solar cell device via scattering from metal or dielectric nanoparticles, with optical confinement provided by the refractive index contrast between the quantum-well layers and surrounding material. Substantially improved current generation and collection over a broad range of wavelengths of incident light is observed, particularly at long wavelengths.

Nominally lattice-matched InP/In_{1-x}Ga_xAs_yP_{1-y} multiple-quantum-well *p-i-n* solar cell structures, shown schematically in Fig. 1(a), were employed in our studies. The *n*-type electrode of all *p-i-n* diode structures consisted of a S doped InP substrate (S concentration $\sim 5 \times 10^{18} \text{ cm}^{-3}$), while the intrinsic region consisted of 10 nm In_{0.91}Ga_{0.09}As_{0.2}P_{0.8} barriers alternating with 10 nm In_{0.81}Ga_{0.19}As_{0.4}P_{0.6} quantum wells for ten periods with an additional 50 nm (device set A) or 25 nm (device set B) In_{0.91}Ga_{0.09}As_{0.2}P_{0.8} barrier above the top quantum-well layer. The *p*-type electrode consisted of a heavily Zn doped (Zn concentration $\sim 3 \times 10^{18} \text{ cm}^{-3}$) 50 nm *p*-type InP layer (set A) or 25 nm *p*-type InP plus 10 nm *p*-type In_{0.47}Ga_{0.53}As (set B). Large-area (typically

1 cm²) *n*-type Ohmic contacts were formed using 40 nm Ti/200 nm Au metallization deposited by electron-beam evaporation. 2 mm² active device window regions were defined by conventional photolithography, and *p*-type contacts were then formed using 20 nm Ti/20 nm Pd/200 nm Au metallization deposited by electron-beam evaporation and a standard lift-off process. The top In_{0.47}Ga_{0.53}As contact layer (device set B only) was then removed from the window region by a selective wet etch (1:10:220 H₂SO₄:H₂O₂:H₂O for 15 s), and an $\sim 15 \text{ nm}$ SiO₂ surface passivation layer was sputter deposited over the active window area of all devices.

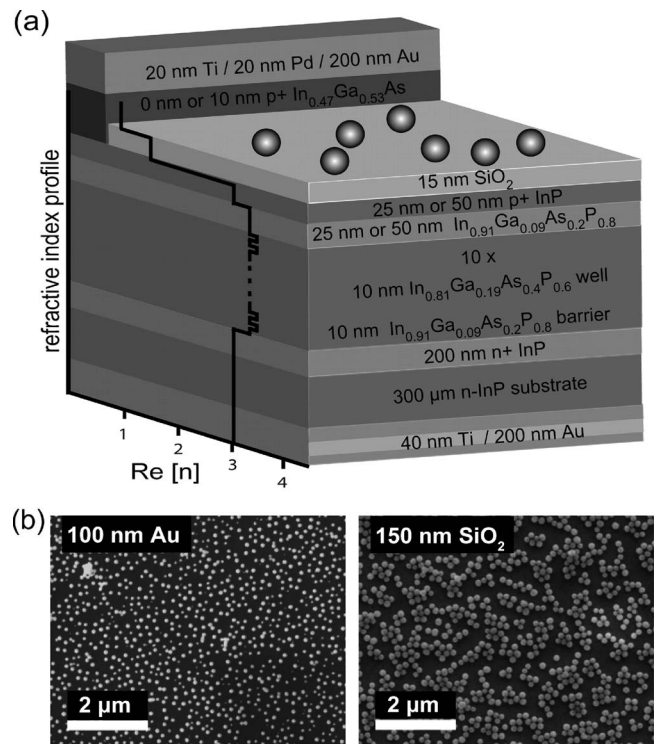


FIG. 1. (a) Schematic of InP-based quantum-well solar cells with nanoparticles on the device surface. Superimposed is the refractive index profile of the quantum-well solar cell. (b) Scanning electron microscope images of 100-nm-diameter Au nanoparticles (left) and 150-nm-diameter SiO₂ nanoparticles (right) deposited on quantum-well solar cell device surfaces (device set B).

^{a)}Present address: Department of Electrical Engineering, University of California, Berkeley, Berkeley, CA 94720.

^{b)}Electronic mail: ety@ece.ucsd.edu.

To optimize collection of photogenerated carriers from the quantum wells and to minimize the reduction in V_{oc} , a sufficiently large electric field across the intrinsic region—on the order of 30 kV/cm or more⁸—is typically required, and the barriers over which the carriers must be thermally or optically excited generally must be 200–450 meV or less.^{8,9} The former condition requires that the intrinsic region in the p - i - n diode be sufficiently thin, while the latter is satisfied by an appropriate choice of quantum-well and barrier materials. For the device structure shown in Fig. 1(a), with an intrinsic layer thickness of 250 nm, the quantum-well electric field is estimated to be 48 kV/cm in equilibrium and 32 kV/cm at a maximum power operating voltage of ~ 0.4 V.

Incorporation of the multiple-quantum-well region, in addition to enabling photon absorption at longer wavelengths, also increases the refractive index within the intrinsic region relative to the surrounding electrode layers,¹⁰ as shown in Fig. 1(a), producing a slab waveguide structure. Indeed, waveguide mode coupling by light scattered from metallic nanoparticles has previously been demonstrated using metal nanoparticles on silicon-on-insulator (SOI) photodetectors.^{11,12} Here, we achieve this scattering effect by deposition of metal or dielectric nanoparticles atop the semiconductor device, as shown in Figs. 1(a) and 1(b). Scattering of incident light by the nanoparticles enables both improved transmission of photons into the semiconductor active layers and coupling of normally incident photons into lateral optically confined paths within the multiple-quantum-well waveguide layer, resulting in increased photon absorption, photocurrent generation, and power conversion efficiency.

Figure 2(a) shows the spectral photocurrent response for an InP homojunction control device, a p -InP/ i -In_{0.91}Ga_{0.09}As_{0.2}P_{0.8}/ n -InP barrier-only control device, and a p - i - n quantum-well solar cell device from device set B. The epitaxial layer structures for the control and quantum-well devices were grown in immediate succession under identical reactor conditions with identical i -layer thicknesses of 225 nm. The photocurrent response for the InP control sample extends only to the InP absorption edge at 960 nm (as determined by room temperature photoluminescence measurements), while for the barrier-only control and quantum-well devices the photocurrent responses extend to the absorption edges of In_{0.91}Ga_{0.09}As_{0.2}P_{0.8} (1040 nm) and In_{0.81}Ga_{0.19}As_{0.4}P_{0.6} (1160 nm), respectively. Figure 2(b) shows the maximum power curves for InP homojunction, p -InP/ i -In_{0.91}Ga_{0.09}As_{0.2}P_{0.8}/ n -InP barrier only, and p - i - n quantum-well solar cell devices from device set A, grown in the same sequential manner as device set B, with i -layer thicknesses of 250 nm. Despite the drop in V_{oc} from 0.63 to 0.64 V for the homojunction and barrier-only devices to 0.53 V for the quantum-well devices, the quantum-well devices exhibit an increase in maximum power output of 7.4% and 4.6% relative to the homojunction and barrier-only devices, respectively.

To illustrate the effectiveness of nanoparticle scattering in improving photocurrent response and power conversion efficiency, we show in Fig. 3 photocurrent response spectra for quantum-well solar cells from device set B with either 100 nm diameter Au or 150 nm diameter SiO₂ nanoparticles deposited on the surface, plotted as ratios relative to the spectrum for the same device without nanoparticles. Surface particle densities of $\sim 2.7 \times 10^9$ and $\sim 2.1 \times 10^9$ cm⁻² were

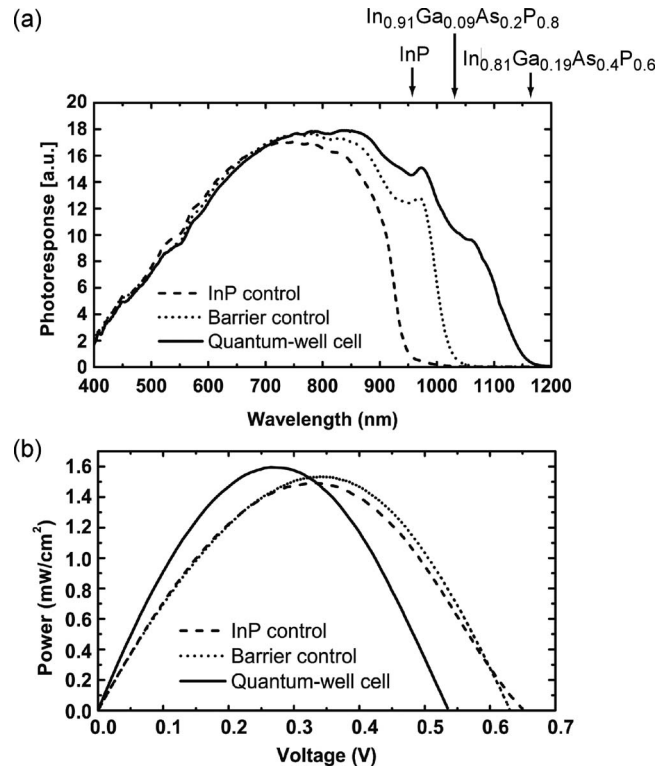


FIG. 2. (a) Photocurrent response spectra for device set B: InP p - i - n control device (dashed line), barrier-material p - i - n control device (dotted line), and p - i - n quantum-well solar cell device (solid line). Absorption edges of InP, In_{0.91}Ga_{0.09}As_{0.2}P_{0.8}, and In_{0.81}Ga_{0.19}As_{0.4}P_{0.6} are indicated. (b) Power output curves for device set A: InP p - i - n control device (dashed line), barrier-only p - i - n control device (dotted line), and p - i - n quantum-well solar cell device (solid line).

employed for Au and SiO₂ nanoparticles, respectively. The nanoparticle deposition procedure and photocurrent measurement apparatus are described in detail elsewhere.^{13,14} Scattering of incident light by Au nanoparticles yields a reduction in photocurrent response at wavelengths of ~ 570 nm and below associated with a phase shift in the scattered wave near the nanoparticle plasmon resonance that results in partial destructive interference between the scattered and the directly transmitted waves.¹³ A broad increase from ~ 570 to > 900 nm arises from strong forward scattering of

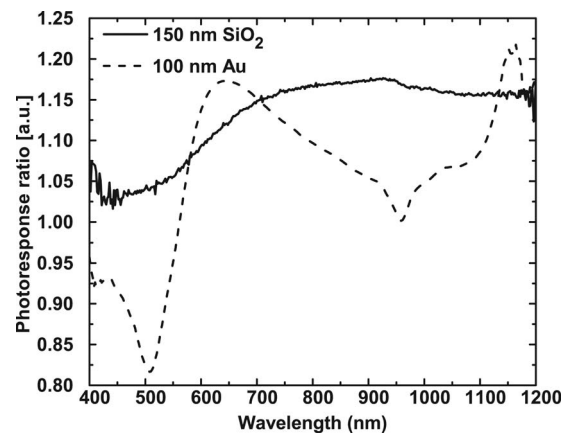


FIG. 3. Photocurrent response spectra of p - i - n quantum-well solar cells from device set B with either 100-nm-diameter Au nanoparticles (dashed line) or 150 nm diameter SiO₂ nanoparticles (solid line) deposited on the surface, plotted as ratios relative to the spectrum for the same devices without nanoparticles.

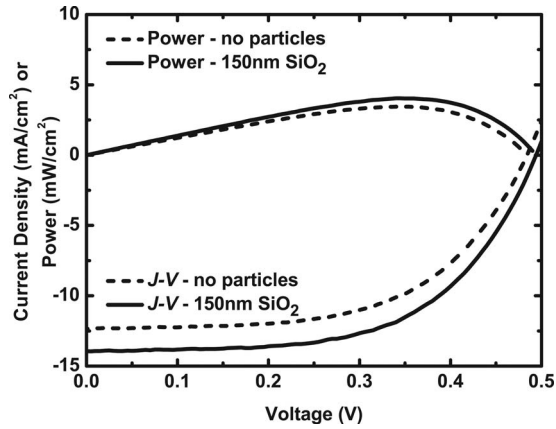


FIG. 4. J - V and output power curves measured for quantum-well solar cell devices (device set B) without SiO_2 nanoparticles (dashed lines) and for the same devices after deposition of 150-nm-diameter SiO_2 nanoparticles (solid lines).

light by the nanoparticles. For the SiO_2 nanoparticles, no surface plasmon polariton resonance is present, and we observe increased transmission and photocurrent response over the entire 400–1200 nm range of wavelengths.¹⁵

For devices functionalized with Au nanoparticles we also observe a pronounced increase in photocurrent response between 960 nm and cutoff at ~ 1200 nm. We attribute this behavior to the scattering of incident radiation into optical propagation modes associated with the slab waveguide formed by the multiple-quantum-well region and surrounding layers. A standard calculation¹⁶ shows that this waveguide supports two confined modes at wavelengths of 960–1200 nm. Furthermore, with increasing wavelength the optical waveguide structure becomes better defined due to the wavelength dependence of the semiconductor refractive indices, resulting in increased coupling efficiency into the guided modes.¹² The improved photocurrent response in this wavelength range then arises because coupling of incident light into the guided and substrate radiation modes leads to a dramatic increase in photon path lengths within the multiple-quantum-well region associated with lateral rather than vertical photon propagation, and consequently greater efficiency in photon absorption.

Previously, our group and others have reported increased J_{sc} and power conversion efficiency due to optical scattering from metal nanoparticles deposited on a -Si solar cells¹⁴ and Si solar cells.^{13,17,18} The enhanced photocurrent response in nanoparticle-functionalized quantum-well solar cells observed here also leads to improved J_{sc} and power conversion efficiency under illumination provided by a Newport 96000 150 W solar simulator with a xenon arc lamp under normal illumination incidence. Figure 4 shows current density-voltage characteristics and the corresponding power output for a quantum-well solar cell from device set B before and after deposition of SiO_2 nanoparticles on the device surface. For a SiO_2 nanoparticle surface density of $\sim 2.1 \times 10^9 \text{ cm}^{-2}$, a 12.9% increase in J_{sc} , an increase in the fill factor from 58% to 59%, and a 17.0% increase in maximum power conversion efficiency were observed. For a Au nanoparticle surface density of $\sim 2.7 \times 10^9 \text{ cm}^{-2}$, a 7.3% increase in J_{sc} and an increase of 1% in maximum power conversion efficiency.

Substantially larger improvements in coupling efficiency and photocurrent enhancement are anticipated for device structures that bound the quantum-well region with a lower refractive index substrate. A model developed by Soller and Hall¹⁹ shows that when a horizontal electric dipole is located above a SOI substrate, an excess of 80% of the light emitted by the dipole is coupled into the supported waveguide modes of the high refractive index guiding Si layer.²⁰ The ratio of the power emitted from the dipole into fully guided modes to the total radiated power of the dipole for our structure over wavelengths ~ 600 –1200 nm occurs with a maximum efficiency $< 10\%$ (although the emission into guided and leaky modes is in the range of 80–90%). This low coupling efficiency is due to the small refractive index contrast inherent to our structure and could be improved in a structure with greater index contrast.

In summary, we have shown that the performance of quantum-well solar cells can be substantially improved by integration of dielectric or metal nanoparticles with the semiconductor device to couple normally incident light into lateral propagation paths confined within the slab waveguide formed by the multiple-quantum-well intrinsic layer. This approach enables the conflict normally inherent in achieving both efficient photon absorption (mandating a thick multiple-quantum-well layer) and efficient collection of photogenerated carriers (typically requiring a thin multiple-quantum-well layer) to be circumvented and could help enable realization of the very high maximum power conversion efficiencies predicted for quantum-well solar cells.

Part of this work was supported by a grant from the UCSD Von Liebig Foundation, by AFOSR (FA9550-07-1-0148), and by DoE (DE-FG36-08GO18016).

¹G. Wei, K. T. Shiu, N. C. Giebink, and S. R. Forrest, *Appl. Phys. Lett.* **91**, 223507 (2007).

²D. Xiangfeng, Y. Huang, Y. Cui, J. Wang, and C. M. Lieber, *Nature (London)* **409**, 66 (2001).

³V. I. Klimov, *Appl. Phys. Lett.* **89**, 123118 (2006).

⁴C. H. Henry, *J. Appl. Phys.* **51**, 4494 (1980).

⁵S. P. Bremner, R. Corkish, and C. B. Honsberg, *IEEE Trans. Electron Devices* **46**, 1932 (1999).

⁶K. W. J. Barnham, B. Braun, J. Nelson, M. Paxman, C. Button, J. S. Roberts, and C. T. Foxon, *Appl. Phys. Lett.* **59**, 135 (1991).

⁷O. Y. Raisky, W. B. Wang, R. R. Alfano, C. L. Reynolds, Jr., D. V. Stampone, and M. W. Focht, *J. Appl. Phys.* **84**, 5790 (1998).

⁸A. Alemu, J. A. H. Coaquira, and A. Freundlich, *J. Appl. Phys.* **99**, 084506 (2006).

⁹J. M. Mohaidat, K. Shum, W. B. Wang, and R. R. Alfano, *J. Appl. Phys.* **76**, 5533 (1994).

¹⁰S. Adachi, *J. Appl. Phys.* **66**, 6030 (1989).

¹¹H. R. Stuart and D. G. Hall, *Appl. Phys. Lett.* **73**, 3815 (1998).

¹²K. R. Catchpole and S. Pillai, *J. Appl. Phys.* **100**, 044504 (2006).

¹³S. H. Lim, W. Mar, P. Matheu, D. Derkacs, and E. T. Yu, *J. Appl. Phys.* **101**, 104309 (2007).

¹⁴D. Derkacs, S. H. Lim, P. Matheu, W. Mar, and E. T. Yu, *Appl. Phys. Lett.* **89**, 093103 (2006).

¹⁵S. P. Sundararajan, N. K. Grady, N. Mirin, and N. J. Halas, *Nano Lett.* **8**, 624 (2008).

¹⁶P. Yeh, *Optical Waves in Layered Media* (Wiley, New York, 1988), p. 319.

¹⁷D. M. Schaadt, B. Feng, and E. T. Yu, *Appl. Phys. Lett.* **86**, 063106 (2005).

¹⁸S. Pillai, K. R. Catchpole, T. Trupke, and M. A. Green, *J. Appl. Phys.* **101**, 093105 (2007).

¹⁹B. J. Soller and D. G. Hall, *J. Opt. Soc. Am. A* **18**, 2577 (2001).

²⁰B. J. Soller, H. R. Stuart, and D. G. Hall, *Opt. Lett.* **26**, 1421 (2001).